



Cite this: DOI: 10.1039/c6dt01310d

Azobenzene-derived tris- β -diketonate lanthanide complexes: reversible *trans*-to-*cis* photoisomerization in solution and solid state†

Li-Rong Lin,^{*a} Xuan Wang,^a Gao-Ning Wei,^a Hui-Hui Tang,^a Hui Zhang^a and Li-Hua Ma^{*b}

Novel azobenzene-derived β -diketonates (4,4,5,5,6,6,6-heptafluoro-1-azobenzene-1,3-hexanedione (**LA**), 4,4,5,5,6,6,6-heptafluoro-1-(4-dimethylamino)azobenzene-1,3-hexanedione (**LB**)) were designed and their complexes with lanthanide cations (La^{3+} , Eu^{3+} , Gd^{3+} , Yb^{3+}) were prepared and characterized by ^1H NMR, FT-IR, and elemental analysis. Three of the complexes were crystallized successfully and identified by X-ray diffraction. It was significant to find that **LA** showed remarkably reversible *trans*-to-*cis* isomerization properties, however, **LB**, bearing an electron donor compared with **LA**, slowed down the isomerization to an extent. The presence of $\text{Ln}(\text{III})$ enhanced the reversible *trans*-to-*cis* isomerization properties of both **LA** and **LB** a little upon photoirradiation in organic solvents, and amazingly increased the fatigue resistance. In addition, the complexes doped in polymethyl methacrylate (PMMA) films produced a similar phenomenon as well as when in solution. Theoretical calculations based on time dependent density functional theory (TD-DFT) were performed for geometry optimization and to determine the excitation energies of **LA** and **LB** to gain further insight into the electronic structure of the complexes, and the data were consistent with the experimental results. The excellent reversible photoisomerization properties of the newly designed $\text{Ln}(\text{III})$ complexes can offer important advantages that will help with the further study of these materials to reach their full potential in applications such as molecular switching devices.

Received 5th April 2016,
Accepted 15th August 2016
DOI: 10.1039/c6dt01310d

www.rsc.org/dalton

Introduction

Azobenzene has received much attention due to its well-known reversible photoisomerization between the *trans* and *cis* isomers.^{1–5} For application of this compound as a bistable molecular photoswitch, a fast switching process, large extinction coefficient with high quantum yield and high fatigue resistance in environmental conditions are important prerequisites.^{3,6,7} For instance, it has been used to orient liquid crystal domains selectively,⁸ create nonlinear optical materials,^{9–11,12–15} change the pitch of a cholesteric phase,¹⁶ incorporate into polymer matrices as stabilizers,^{17–20,21–23} and

control protein activity by attaching ligands to photomodulate their affinity.^{24–27} Most importantly, it is perhaps the best artificial mimic of the retinal/rhodopsin photoswitch system in terms of reversibility, speed and simplicity of incorporation.²⁸ However, this emerging field is at an early stage of research output, and the utility of azobenzene is still limited. Extension of the photoresponsive azobenzene to metal complexes results in substantial functions, in view of the combination of optical, magnetic, redox and other unexpected properties of the azobenzene moiety, and is an interesting alternative to pure azobenzene.^{29–31} A number of photoisomerization azo-attached metal complexes have been reported in recent years, including a wide range of metal centers such as Cr,³² Cu,³³ Co,³⁴ Fe,^{34–36} Zn,^{33,37} Ir,³⁸ Ru,^{39,40} Rh,^{39,40} and Pt.⁴¹ There is a good review that covers the primary studies.⁴² Data related to the lanthanide ions ($\text{Ln}(\text{III})$) that possess unusual electronic properties that result from shielding of the 4f orbitals by the filled 5s² and 5p⁶ sub-shells are barely reported.⁴³

Nevertheless, $\text{Ln}(\text{III})$ complexes with β -diketonates are stable in aqueous solutions since diketonate ligands have the advantage of a negatively charged binding site that leads to neutral, 3 : 1 ligand : lanthanide complexes.⁴⁴ Lanthanide diketonate complexes have been widely studied as highly luminescent

^aDepartment of Chemistry, College of Chemistry and Chemical Engineering, Xiamen University, Xiamen, 361005, P. R. China. E-mail: linlr@xmu.edu.cn

^bDepartment of Chemistry, School of Science and Computer Engineer, University of Houston at Clear Lake, 2700 BAY AREA BLVD, Houston, TX, 77058, USA. E-mail: MaL@UHCL.edu

† Electronic supplementary information (ESI) available: X-ray crystallographic files for complexes $\text{Yb}(\text{LA})_3$, $\text{Eu}(\text{LB})_3$ and $\text{Yb}(\text{LB})_3$ in CIF format, Fig. S1–S22, the *trans*-*cis* photoisomerization kinetics curves (Fig. S23–S33), NMR spectra for ligands and complexes (Fig. S34–S43), and IR spectra for all complexes (Fig. S44–S53). CCDC 1422641–1422643. For ESI and crystallographic data in CIF or other electronic format see DOI: 10.1039/c6dt01310d

materials,^{45–49} effective receptors for anionic substrates^{50–53} and chiral sensing,^{54,55} and even more for the development of new materials as second-order nonlinear optical chromophores,⁵⁶ near-IR LEDs^{57,58} or polymers.⁵⁹ Carbon–fluorine (C–F) has commonly been introduced to the molecular system as part of the lanthanide ligands because it is a highly electron-withdrawing group, which can minimize the energy losses and better promote the solubility of lanthanide bis(β -diketonate) complexes in different organic solvents.^{45,46} In the studied Ln(III) complexes with β -diketonates, the direct absorption of Ln(III) is weak due to their Laporte forbidden f–f transitions, and energy transfer from the chromophore to the metal center usually takes place to modulate their luminescence properties.⁶⁰ We then designed and synthesized two novel ligands which incorporated an azo group into the β -diketone derivatives. We synthesized 4,4,5,5,6,6,6-heptafluoro-1-azobenzene-1,3-hexanedione (**LA**) and 4,4,5,5,6,6,6-heptafluoro-1-(4-dimethylamino)azobenzene-1,3-hexanedione (**LB**). **LA** and **LB** contained the same azo group but with different electron donating abilities. We presented the structural characterization of **LA** and **LB** in combination with the Ln(III) cations.

We investigated the reversible *trans*-to-*cis* photoisomerization of these azobenzene-derived tris- β -diketonate Ln(III) complexes. Unsurprisingly, the luminescence properties of the complexes were not obvious as the energy could not be transferred from the chromophore to the metal center. The excitation energies of the lowest excited triplet states of **LA** and **LB** were calculated by time-dependent density functional theory (TD-DFT) to be 1.7215 and 1.7025 eV, respectively. Both of these were lower than the resonance level of the Eu³⁺ (⁵D₀, 2.1434 eV) and Gd³⁺ (⁶P_{7/2}, 3.9957 eV) ions. Thus, the excitation energy could not be transferred from the ligands to the rare earth ions according to the triplet state of the ligand that was below the resonance level of the rare earth ion. Nevertheless, the coordination effect of Ln(III) to the ligands increased the rate of *trans*-to-*cis* photoisomerization of the azo ligands, as well as the fatigue resistance as a consequence of the parity forbidden nature of the 4f transitions. The *trans*-to-*cis* photoisomerization rate constants of our complexes for the **LA** ligand (10^{-2} s⁻¹) are at least 10 times higher than the reported Ru(II), Rh(III) and Ir(III) complex (10^{-5} – 10^{-3} s⁻¹), as well as azobenzene itself (10^{-5} – 10^{-4} s⁻¹).^{39,41,61}

To the best of our knowledge, this is the first report of the synthesis of **LA** and **LB** and their complexing behavior with Ln(III) ions in both liquid (organic solvents) and solid (poly-methyl methacrylate (PMMA) film) statuses.

Results and discussion

Characterization and X-ray crystallographic analysis

The eight azobenzene-derived tris- β -diketonate lanthanide complexes are soluble in most polar solvents, such as acetonitrile, dichloromethane and chloroform. All of them contain two water molecules characterized by elemental analyses and thermal analysis. The thermal properties of the eight

complexes were examined using thermogravimetric analysis (TGA) in the temperature range of 30–900 °C on powder samples, and the TGA results are shown in Fig. 1. As expected, the **LA**-Ln(III) complexes have similar thermal behavior, so do the **LB**-Ln(III) complexes. However, a remarkable difference is observed between **LA**-Ln(III) and **LB**-Ln(III), which could be ascribed to the *N,N*-dimethyl substituted group on the azobenzene. The melting points of complexes **LB**-Ln(III) are higher than those of complexes **LA**-Ln(III). This is easy to understand because the *N,N*-dimethyl substituted group leads to higher melting points.⁶² From the TGA traces, it is obvious that the two groups have very similar weight loss trends. A weight loss of about 2.48–2.87% before 97 °C can be observed for complexes **LA**-Ln(III), whereas complexes **LB**-Ln(III) lose 2.25–2.39% weight before 133 °C, suggesting that all the complexes lose two water molecules at this step. Then complexes **LA**-Ln(III) and **LB**-Ln(III) reach constant weights until 240 °C and 273 °C, respectively. Upon further heating, they start to decompose until 900 °C.

The crystal structures of Yb(**LA**)₃, Eu(**LB**)₃ and Yb(**LB**)₃ were obtained by slow evaporation of their methanol and ethanol or ethanol and acetone mixed solutions for two weeks to give plate crystals, which were determined by single-crystal X-ray crystallography. All three complexes crystallize in the triclinic *P* $\bar{1}$ space group with two molecules in each unit cell. They have very similar structures with three ligands and two solvent molecules coordinated in each asymmetric unit, corresponding to a formula of [Ln(L)₃](Solvent)₂. Crystallographic details are shown in Table 1. The crystal of complex Yb(**LA**)₃ is formed by the chelation of three **LA** ligand anions and two ethanol molecules substituting its original two water molecules. The Yb(III) ion is eight-coordinated to six oxygen atoms from the three **LA** ligands and two oxygen atoms from solvent ethanol, forming a trigonal dodecahedron coordination geometry (Fig. 2). The crystal structures of complexes Eu(**LB**)₃ and Yb(**LB**)₃ are isomorphic with that of complex Yb(**LA**)₃. The differences among them are in the coordinated solvent molecules. For complex Eu(**LB**)₃, the Eu(III) ion is eight-coordinated to six oxygen atoms from the three **LB** ligands and two oxygen atoms from one solvent ethanol and one water, and the unit cell contains two solvent acetone molecules (Fig. S1 in the ESI†). The oxygen atom from the acetone molecule forms intermolecular hydrogen bonding both with the hydrogen

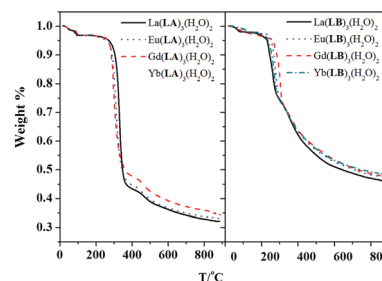


Fig. 1 TGA curves of complexes **LA**-Ln(III) and **LB**-Ln(III).

Table 1 Crystallographic data for complexes Yb(LA)₃, Eu(LB)₃ and Yb(LB)₃

Crystal data	Yb(LA) ₃ (CH ₃ CH ₂ OH) ₂	Eu(LB) ₃ (CH ₃ CH ₂ OH)(H ₂ O)	Yb(LB) ₃ (CH ₃ CH ₂ OH) ₂
CCDC number	1422642	1422641	1422643
Empirical number	C ₅₈ H ₄₂ F ₂₁ N ₆ O ₈ Yb	C ₆₂ H ₅₃ F ₂₁ N ₉ O ₈ Eu, 2(C ₃ H ₆ O)	C ₆₄ H ₅₇ F ₂₁ N ₉ O ₈ Yb, H ₂ O
Formula weight	1523.01	1719.25	1670.24
Temperature (K)	173	173	173
Wavelength (Å)	0.71073	0.71073	0.71073
Crystal system	Triclinic	Triclinic	Triclinic
Space group	<i>P</i> $\bar{1}$	<i>P</i> $\bar{1}$	<i>P</i> $\bar{1}$
<i>a</i> (Å)	11.023(15)	10.143(5)	10.786(10)
<i>b</i> (Å)	11.338(16)	14.054(7)	13.663(12)
<i>c</i> (Å)	23.45(3)	26.70(1)	23.76(2)
α (°)	90.46(1)	92.08(1)	84.22(13)
β (°)	99.96(1)	96.84(1)	89.38(15)
γ (°)	93.35(1)	108.54(1)	74.27(5)
<i>V</i> (Å ³)	2881(7)	3571(3)	3353(6)
<i>Z</i>	2	2	2
Calculated density (mg m ⁻³)	1.756	1.599	1.653
Absorption coefficient (mm ⁻¹)	1.753	0.996	1.516
θ range	2.19 to 23.95	1.5 to 25.0	0.86 to 28.11
Reflections collected	14 618	25 803	29 138
Completeness to theta	98.7%(25.00°)	99.0%(25.00°)	99.0%(25.23°)
Data/restraints/parameters	9945/7/870	12 596/20/1083	15 071/46/977
Goodness of fit on <i>F</i> ²	0.995	1.149	1.025
Final <i>R</i> indices [<i>I</i> > 2 σ (<i>I</i>)]	<i>R</i> ₁ = 0.0648 <i>wR</i> ₂ = 0.1657	<i>R</i> ₁ = 0.0611 <i>wR</i> ₂ = 0.1541	<i>R</i> ₁ = 0.0900 <i>wR</i> ₂ = 0.2241
<i>R</i> indices (all data)	<i>R</i> ₁ = 0.0820 <i>wR</i> ₂ = 0.1578	<i>R</i> ₁ = 0.0692 <i>wR</i> ₂ = 0.1504	<i>R</i> ₁ = 0.151 <i>wR</i> ₂ = 0.2624

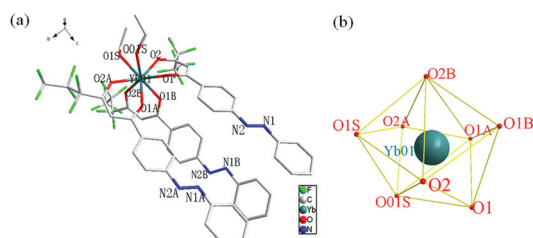


Fig. 2 Crystal structure of Yb(LA)₃(CH₃CH₂OH)₂ (all hydrogen atoms are omitted for clarity) (a) and the coordination polyhedron geometry of the central Yb(III) (b). Selected bond distances (Å) and angles (°): YbO1–O1A 2.210(6), YbO1–O2 2.226(5), YbO1–O2B 2.218(6), YbO1–O1B 2.259(6), YbO1–O1 2.283(6), YbO1–O2A 2.294(6), YbO1–O01S 2.363(7), YbO1–O1S 2.371(6); O1A–YbO1–O2B 93.6(2), O1A–YbO1–O1B 74.0(2), O2B–YbO1–O1 147.1(2), O1B–YbO1–O1 74.2(2), O2–YbO1–O2A 144.6(2), O1–YbO1–O2A 126.8(2), O2–YbO1–O01S 94.0(2), O1–YbO1–O01S 72.9(2).

atom from the coordinated water molecule and the ethanol hydroxyl (O1W–H2W...O–1S 2.643 Å, O2C–H2C...O2S 2.762 Å). For complex Yb(LB)₃, the Yb(III) ion is also eight-coordinated to six oxygen atoms from the three LB ligands and two oxygen atoms from the two solvent ethanol, and the unit cell contains one solvent water molecule (Fig. S2 in the ESI[†]). The oxygen atom from the solvent water molecule forms intermolecular hydrogen bonding with the hydrogen atom from the coordinated ethanol hydroxyl (O9–H9B...O8 2.770 Å). The Yb–O distances are found in the ranges of 2.212(6)–2.371(6) Å for Yb(LA)₃ and 2.229(8)–2.344(10) Å for Yb(LB)₃, and the Eu–O bond lengths are in the range of 2.316(4)–2.464(4) for Eu(LB)₃; all are in the normal ranges compared with other lanthanide β -diketonates complexes reported.⁴⁴

UV-vis spectroscopy

The absorption spectra of the free ligands LA, LB and their complexes LA–Ln(III), LB–Ln(III) in acetonitrile solution at room temperature are shown in Fig. 3, and the spectral data are presented in Table 2. When changing the organic solvents to ethanol and hexane, the spectral behavior of these compounds are very similar to that in acetonitrile (Fig. S3 and S4 in the ESI[†]). As shown in Fig. 3, the free LA ligand has typical absorption bands of azobenzene derivatives in the region of 300–500 nm, a high intensity π – π^* band (358 nm/ 3.74×10^5 L mol⁻¹ cm⁻¹) and a low intensity n – π^* band (443 nm/ 850 L mol⁻¹ cm⁻¹), whereas LB has only high intensity π – π^* bands (273 nm/ 2.49×10^4 , 332 nm/ 3.19×10^4 , 489 nm/ 9.53×10^4 L mol⁻¹ cm⁻¹) due to the contribution of the electron-donating *N,N*-dimethylamino group. The large red shift of the π – π^*

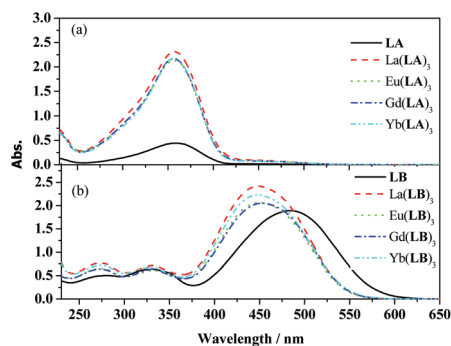


Fig. 3 Absorption spectra of LA, LA–Ln(III) (a) and LB, LB–Ln(III) (b) (2.0×10^{-5} mol L⁻¹) in acetonitrile solution.

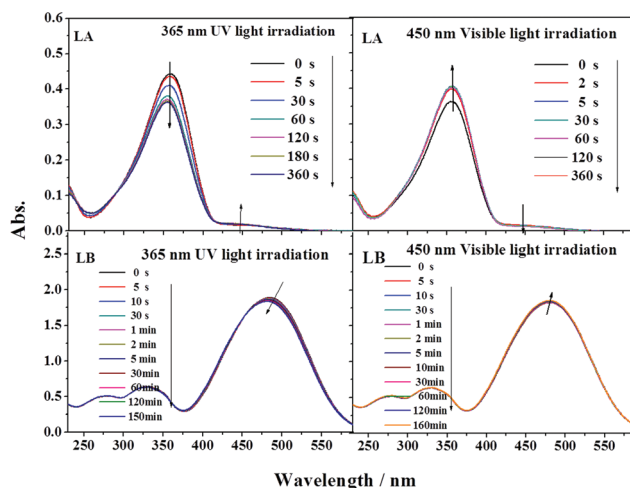
Table 2 UV-vis absorption data of ligands **LA** and **LB** and complexes **LA-Ln(III)**, **LB-Ln(III)** in different solvents (λ_{\max} [nm], ϵ_{\max} [10^4 L mol $^{-1}$ cm $^{-1}$] in brackets)

Compounds	Acetonitrile	Ethanol	Hexane
LA	358(3.74), 446(0.085)	356(3.32), 452(0.080)	357(6.15), 452(0.14)
La(LA)₃	358(11.56), 446(0.46)	357(10.09), 454(0.44)	357(13.07), 450(0.32)
Eu(LA)₃	358(10.68), 446(0.42)	357(10.11), 454(0.41)	357(9.70), 450(0.31)
Gd(LA)₃	358(10.85), 446(0.38)	357(10.27), 454(0.37)	357(11.76), 450(0.31)
Yb(LA)₃	358(10.86), 446(0.37)	357(11.14), 454(0.36)	357(10.49), 450(0.28)
LB	273(2.49), 332(3.19), 489(9.53)	273(2.74), 332(2.77), 462(7.85)	368(1.11), 320(1.31), 452(4.34)
La(LB)₃	273(3.89), 332(3.58), 451(12.06)	273(3.78), 332(3.30), 443(11.67)	270(3.17), 330(3.17), 433(9.36)
Eu(LB)₃	273(3.28), 332(3.07), 451(10.22)	273(2.70), 332(2.37), 443(8.34)	273(2.79), 330(2.88), 436(6.97)
Gd(LB)₃	273(3.18), 332(3.21), 451(10.22)	273(2.96), 332(2.76), 443(9.36)	273(2.71), 330(3.03), 443(6.85)
Yb(LB)₃	273(3.59), 332(3.44), 451(11.13)	273(2.99), 332(2.87), 443(9.12)	271(2.92), 330(3.17), 435(8.87)

band (489 nm) of **LB** leads to no observation of the weak $n-\pi^*$ band, perhaps because the $n-\pi^*$ band is buried in the absorption band at 489 nm.² The absorption spectra of the **LA-Ln(III)** complexes show similar absorption bands to those of free ligand **LA** in different solvents such as acetonitrile, ethanol and hexane, with a high intensity band at around 350 nm and a low intensity $n-\pi^*$ band at around 450 nm. The difference between the **LA-Ln(III)** complexes and pure ligand **LA** is that the molar extinction coefficients of the **LA-Ln(III)** complexes are nearly five times stronger than that of **LA**. This is easily reasoned by the ligand absorption being perturbed by the lanthanide ion coordination, as expected, and it is proportional to the number of azobenzene β -diketones in the complex. In the case of **LB** and the **LB-Ln(III)** complexes, lanthanide ion coordination produces a large bathochromic shift in the intense $\pi-\pi^*$ band at around 451 nm. This observation suggests that the *para* electron-donating *N,N*-dimethylamino group makes the **LB** ligand push-pull an azobenzene derivative. As a result, **LB** presents an intense and red shifted $\pi-\pi^*$ band at around 451 nm, which buries its $n-\pi^*$ band. Lanthanide ions coordinate to such a push-pull ligand and establish stronger electronic communication to the azobenzene group, leading to the large bathochromic shift in the intense $\pi-\pi^*$ band.

Photoisomerization behavior of **LA** and **LB**

The change of the UV-vis absorption spectra of the **LA** and **LB** ligands upon irradiation with UV (365 nm) and visible (450 nm) light in acetonitrile solution as a function of time is shown in Fig. 4. Similar absorption spectra in ethanol and hexane solutions are in the ESI (Fig. S5–S8†). For **LA**, upon UV 365 nm light irradiation, the absorbance at 358 nm due to the symmetry-allowed $\pi-\pi^*$ transition decreases, while the absorbance at 446 nm due to the symmetry-forbidden $n-\pi^*$ transition increases. The absorption spectrum of the photo-stationary state appears after 30 min. Subsequent irradiation with visible (450 nm) light leads to partial complete recovery of the absorption spectrum. This reversible spectral change was observed repeatedly, indicating the absorption spectrum change upon irradiation results from the photoisomerization of the azobenzene group. The UV-vis spectrum of **LB** upon UV 365 nm light irradiation exhibits a decrease in the high

**Fig. 4** UV-vis spectral changes of **LA** and **LB** in acetonitrile (2.0×10^{-5} mol L $^{-1}$) upon irradiation at 365 nm and recoverable irradiation at 450 nm as a function of time.

intensity band at 489 nm and is accompanied by a slightly bathochromic shift to 485 nm, owing to the *trans*-to-*cis* photoisomerization. The back reversion of *cis*-to-*trans* isomerization upon visible light irradiation is also observed. Measuring the degree of photoisomerization by ^1H NMR was unsuccessful due to the overlap of signals, however, an estimate of the photoreaction yields can be made. The quantum yields ($\Phi_{t \rightarrow c}$) in different solvents are evaluated using eqn (1), see the Experimental section. The quantum yields ($\Phi_{t \rightarrow c}$) of **LA** and **LB** in different solvents are listed in Table 3. It is obvious that **LA** exhibits higher quantum yields and conversion ratios for *cis*-to-*trans* photoisomerization than **LB**. Here, the *para* electron-donating *N,N*-dimethylamino group produces drastic changes to the absorption and undesired photochemical properties of **LB**.

Photoisomerization behavior of complexes **LA-Ln(III)** and **LB-Ln(III)** in different solvents

Complexes **LA-Ln(III)** and **LB-Ln(III)** derived from ligands **LA** and **LB** showed similar spectral changes upon irradiation in different solvents. However, the rates of the isomerization

Table 3 Quantum yields ($\Phi_{t \rightarrow c}$) and rate constants of the photoisomerization of **LA** and **LB** and complexes **LA**-Ln(III) and **LB**-Ln(III) in different solvents

Compounds	Acetonitrile $\Phi_{t \rightarrow c}$, $10^2 k_{iso}$ [s ⁻¹]	Ethanol $\Phi_{t \rightarrow c}$, $10^2 k_{iso}$ [s ⁻¹]	Hexane $\Phi_{t \rightarrow c}$, $10^2 k_{iso}$ [s ⁻¹]
LA	0.25 ± 0.02, 0.32 ± 0.03	0.17 ± 0.02, 0.22 ± 0.02	0.021 ± 0.002, 0.85 ± 0.06
La(LA) ₃	0.21 ± 0.02, 1.70 ± 0.10	0.23 ± 0.02, 1.30 ± 0.08	0.13 ± 0.01, 0.75 ± 0.04
Eu(LA) ₃	0.19 ± 0.02, 0.11 ± 0.02	0.19 ± 0.02, 0.91 ± 0.03	0.10 ± 0.01, 0.56 ± 0.05
Gd(LA) ₃	0.16 ± 0.02, 0.85 ± 0.05	0.17 ± 0.02, 0.91 ± 0.04	0.10 ± 0.01, 0.85 ± 0.04
Yb(LA) ₃	0.14 ± 0.02, 0.98 ± 0.05	0.17 ± 0.02, 0.91 ± 0.03	0.19 ± 0.02, 0.92 ± 0.05
LB	0.0034 ± 0.0005, 0.21 ± 0.02	—	—
La(LB) ₃	—	—	0.0086 ± 0.0001, 0.013 ± 0.02
Eu(LB) ₃	0.0035 ± 0.0005, 0.34 ± 0.03	0.010 ± 0.005, 0.87 ± 0.08	0.080 ± 0.007, 2.90 ± 0.10
Gd(LB) ₃	0.00093 ± 0.0002, 0.074 ± 0.007	0.017 ± 0.0007, 1.40 ± 0.08	0.024 ± 0.003, 2.10 ± 0.10
Yb(LB) ₃	0.0054 ± 0.001, 0.67 ± 0.06	0.0018 ± 0.0002, 0.83 ± 0.04	0.049 ± 0.005, 0.22 ± 0.02

— No significant photoisomerization behavior was observed.

processes are different in organic solvents as listed in Table 3. For example, the rate of Eu(**LA**)₃ in acetonitrile differs by an order of magnitude *vs.* in ethanol, and the rate of Gb(**LB**)₃ in acetonitrile also is higher than that in ethanol and hexane. There are two possible reasons for the phenomena, one is that the dielectric constant of acetonitrile is relatively larger (36.8),⁶³ the other is related to the physical properties of the lanthanides. Both Eu(III) and Gd(III) have a higher number of single f electrons. For example, Eu(III) has an electron configuration of f⁶. The six electrons are unpaired, each in a different singly occupied f-orbital. Gd(III) contains seven single f electrons. While there is no f electron for La(III), Yb only has one unpaired electron within 13 f electrons. Compared with other azobenzene-containing organometallic compounds, such lanthanide coordinated complexes show active photoisomerization.³⁹ Their photoisomerization quantum yields are comparable and even better than the pure ligands. It is obvious that the *trans*-to-*cis* photoisomerization rates of our complexes derived from the **LA** ligand (10⁻² S⁻¹) are at least 10 times higher than the reported complex (10⁻⁵-10⁻³ S⁻¹), as well as azobenzene itself (10⁻⁵-10⁻⁴ S⁻¹).^{39,41,61} Taking complexes Yb(**LA**)₃ and Yb(**LB**)₃ as examples, Fig. 5 shows the typical spectral change of Yb(**LA**)₃ in acetonitrile solution upon 365 nm irradiation and its recoverable spectrum after 450 nm irradiation. The absorption maximum of Yb(**LA**)₃ in acetonitrile appears at 358 nm, characteristic of the π-π* absorption

band, and there is a very weak n-π* absorption band at 446 nm. Upon UV irradiation, a band at 446 nm develops at the expense of the original band at 358 nm, accompanied by a slightly bathochromic shift to 349 nm with three isosbestic points located at 233, 288 and 413 nm. This is a spectral indication of the occurrence of photoisomerization in solution. The photoisomerization of Yb(**LA**)₃ in solution obeys the first-order reaction with the rate constants of 9.8 × 10⁻² s⁻¹ in acetonitrile, 9.1 × 10⁻² s⁻¹ in ethanol and 9.2 × 10⁻² s⁻¹ in hexane, respectively (Table 3). It reached a photostationary state in 10 min with irradiation at 365 nm. When the UV irradiation ceased, the compound turned back to 80% *trans* form with visible 450 nm irradiation in 10 s. The reason for the incomplete recovery of the *trans* form by visible light is that it reaches a photostationary state. The photochemical pathway is not simple in such a complex, as visible absorption would involve mixing of other bands such as LMCT bands, not just the azo n-π* band. The good reversibility of the *trans*-*cis*-*trans* photoisomerization of Yb(**LA**)₃ in acetonitrile denied the possibility of photodegradation (Fig. S9†). To test the stability of the *trans*-*cis*-*trans* photoisomerization, ten cycles of complex Yb(**LA**)₃ switching in acetonitrile were conducted by irradiating the sample using 365 nm light for 10 min, followed by 450 nm light for 2 min. The complex Yb(**LA**)₃ was stable under these conditions and no signs of photodegradation were detected. The excellent photostability of the complex is vivid for a sustainable application as a molecular photoswitch. The UV-vis absorption spectral changes of Yb(**LA**)₃ in ethanol and hexane solutions are similar to those in acetonitrile (Fig. S10 and S11 in the ESI†), and complexes La(**LA**)₃, Eu(**LA**)₃, and Gd(**LA**)₃ have similar UV-vis absorption spectra changes to that of Yb(**LA**)₃ (Fig. S12-S14 in the ESI†). Complexes **LA**-Ln(III) show overall reversible isomerization reactions and more than ten cycles can be repeated, demonstrating their excellent fatigue resistance and reversibility.

The UV-vis spectral changes of Yb(**LB**)₃ upon UV 365 nm light irradiation in acetonitrile exhibit a similar trend as that of **LB**, decreasing in the high intensity band at 451 nm and being accompanied by a slightly bathochromic shift to 445 nm, owing to the *trans*-to-*cis* photoisomerization (Fig. S15†). As shown in Table 3, the quantum yield of

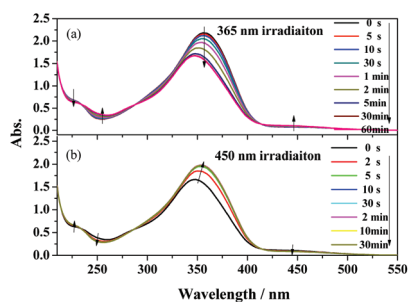


Fig. 5 UV-vis spectral changes of Yb(**LA**)₃ in acetonitrile (2.0 × 10⁻⁵ mol L⁻¹) upon irradiation at 365 nm and recoverable irradiation at 450 nm as a function of time.

isomerization of Yb(LB)₃ is much smaller than that of LA and the LA–Ln(III) complexes due to the *para* electron-donating *N,N*-dimethylamino group in the LB ligand. The photoisomerization properties of complexes La(LB)₃, Eu(LB)₃, Gd(LB)₃ are similar to those of Yb(LB)₃ (Fig. S16–S19 in the ESI†).

Photoisomerization behavior of the LA–Ln(III) complexes in PMMA film

The LA–Ln(III) complexes showed nice reversible and repeated isomerization reactions in solution. For the purpose of practical use, we extended the system from organic solvents to the solid state. Therefore, the LA–Ln(III) complexes in solid PMMA film were investigated. The transmittance absorption spectrum changes of LA–Ln(III) doped in PMMA film upon photoirradiation were measured. The four complexes showed even more excellent reversible and repeated isomerization reactions in PMMA film than those in solution. Fig. 6 shows the UV–vis

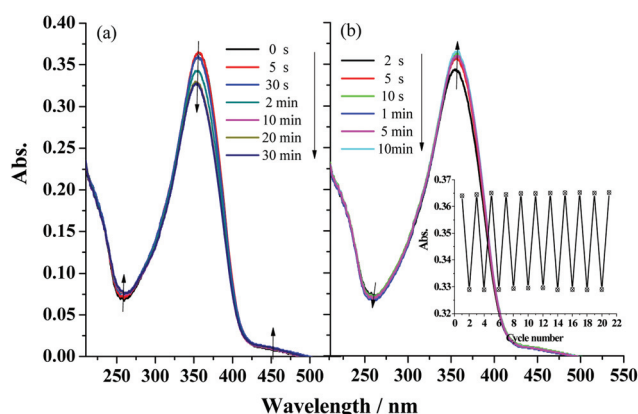


Fig. 6 UV–vis spectral changes of Yb(LA)₃ in PMMA film (5.0 wt%) upon irradiation at 365 nm (a) and recoverable irradiation at 450 nm as a function of time (b) (inset: reversible change of the absorption intensity at 358 nm in the photostationary states after alternating the irradiation at 365 nm and 450 nm in repeating switching cycles).

Table 4 *Trans*-to-*cis* photoisomerization rate constants of the LA–Ln(III) complexes in PMMA film

Compounds	La(LA) ₃	Eu(LA) ₃	Gd(LA) ₃	Yb(LA) ₃
$10^3 k_{\text{iso}} (\times \text{s}^{-1})$	$4.8 \pm 1.9\%$	$6.2 \pm 1.2\%$	$3.3 \pm 9.7\%$	$3.4 \pm 4.4\%$

Table 5 Excited states of molecular LA and LB

LA				LB			
Excited state	Multiplicity	Excited energy/eV	Oscillator strengths	Excited state	Multiplicity	Excited energy/eV	Oscillator strengths
1	T	1.7215	0.0000	1	T	1.7025	0.0000
2	T	2.0726	0.0000	2	T	1.8160	0.0000
3	T	3.1669	0.0000	3	T	2.8224	0.0000
4	S	2.4199	0.0000	4	S	2.4466	0.0000
5	S	3.4404	0.9958	5	S	2.6755	0.7962
6	S	3.5672	0.0003	6	S	3.0850	0.3377

absorption spectral changes of Yb(LA)₃ in PMMA film upon irradiation at 365 nm and its recoverable spectral changes upon irradiation at 450 nm. The π – π^* absorption band of Yb(LA)₃ in PMMA film also appears at 358 nm, and there is a weak n – π^* absorption band at 446 nm. Upon 365 nm UV irradiation, the band at 446 nm is developed at the expense of the band at 358 nm, and is accompanied by a slightly bathochromic shift to 348 nm with three isosbestic points at 233, 288 and 413 nm. The first-order reaction rate constant of Yb(LA)₃ in PMMA film is $3.3 \times 10^{-3} \text{ s}^{-1}$. It reaches a photostationary state in just 10 min with irradiation at 365 nm. When the UV irradiation ceases, the system almost completely returns to the *trans* form with visible 450 nm irradiation in 10 s. The complete recovery of the *trans* form by visible light demonstrates that the photochemical pathway is simple in the solid state. To test the stability of the *trans*–*cis*–*trans* photoisomerization, ten cycles of Yb(LA)₃ switching in PMMA film were conducted by irradiating the sample using 365 nm light for 10 min, followed by 450 nm light for 1 min. Complex Yb(LA)₃ in PMMA film was very stable under these conditions and no signs of photodegradation were detected. The other three complexes, La(LA)₃, Eu(LA)₃ and Gd(LA)₃, have similar isomerization properties to those of Yb(LA)₃ (Fig. S20–S22 in the ESI†). The first-order reaction rate constants of LA–Ln(III) in PMMA film are listed in Table 4. The excellent photostability of the complexes is vivid for future application in molecular switching devices.

TD-DFT calculations

The geometry of the ground states of LA and LB in gas were optimized by the DFT(B3LYP) method with the 6-31+G(d) basis set. TD-DFT was then applied to calculate their excitation energies and the oscillator strengths of the singlet and triplet states. The data are summarized in Table 5. The excitation energies of the lowest excited triplet states of LA and LB are 1.7215 and 1.7025 eV, respectively, and both are lower than the resonance level of the Eu³⁺ (⁵D₀, 2.1434 eV) and Gd³⁺ (⁶P_{7/2}, 3.9957 eV) ions, which is the major reason that the luminescence properties of the LA–Ln(III) and LB–Ln(III) complexes are not obvious. The energy could not be transferred from the chromophore to the metal center. Moreover, the oscillator strength of the lowest excitation energy of the singlet transition of both LA and LB is calculated to be 0,

indicating a disallowed transition. Meanwhile the oscillator strength of the second singlet transition state is near to 1, the ligand is mainly excited to the second singlet transition state, and then relaxes to the lowest energy singlet transition or to the ground state, which also hinders the energy transfer from ligands to the lanthanide ions. Thus, the excitation energy could not be transferred from the ligand to the rare earth ion according to the triplet state of the ligand that was below the resonance level of the rare earth ion.⁶⁴ Therefore, it is easy to understand why the luminescence properties were not observed in the Eu^{3+} and Gd^{3+} complexes at room temperature. Currently, further studies focusing on the construction of novel lanthanide complexes with azo derived β -diketones showing luminescence and photoisomerization dual-behavior are being considered in our laboratory.

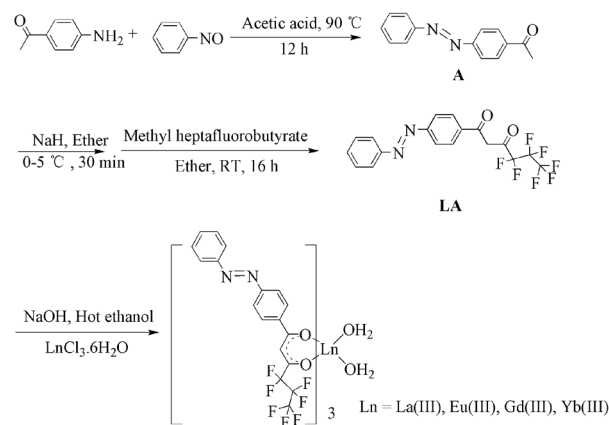
Experimental

Materials and methods

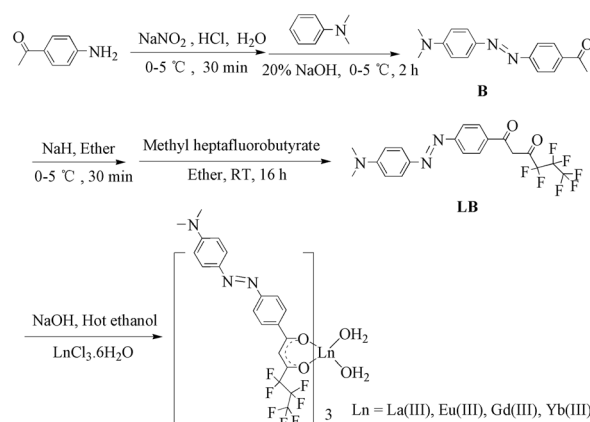
$\text{LnCl}_3 \cdot 6\text{H}_2\text{O}$ ($\text{Ln} = \text{La}, \text{Eu}, \text{Gd}$ and Yb ; Jinan Camolai Trading Company), methyl heptafluorobutyrate (TCI (Shanghai) Chemical Industry Co.), polymethyl methacrylate (PMMA) (Alfa Aesar) and all other chemicals were obtained from Sinopharm Chemical Reagent Co. Analytical-grade solvents were all received from Shanghai Chemicals Group Co. and were redistilled before use, except for ether and tetrahydrofuran, which were freshly prepared by distilling a deep-blue solution resulting from benzophenone/sodium under dry dinitrogen before use. The melting point was determined with an X-4 micromelting point apparatus without correction. Elemental analyses were performed on a Vario EL III elemental analyzer. Infrared spectra were recorded on a Nicolet AVATAR FT-IR 330 spectrometer by using pressed KBr pellets in the range of $4000\text{--}400\text{ cm}^{-1}$. Absorption spectra were scanned using a Shimadzu UV-2550 absorption spectrophotometer. ESI-MS data were obtained on a Bruker ESQUIRE-3000 Plus LC-MS/MS spectrometer. Solution ^1H NMR spectra were acquired on a Bruker Unity 400 MHz (or 500 MHz) spectrometer using TMS as an internal standard. Thermogravimetric analysis (TGA) was carried out on a SDTQ 600 thermogravimeter at a heating rate of $10\text{ }^\circ\text{C min}^{-1}$ under a dinitrogen atmosphere.

Ligand synthesis (see Schemes 1 and 2)

Synthesis of 4-acetyl-azobenzene (A).⁶⁵ Nitrosobenzene (0.16 g, 1.5 mmol) was dissolved in 6 ml of acetic acid and heated to $90\text{ }^\circ\text{C}$, then 0.18 g 1-(4-aminophenyl)ethanone (1.5 mmol) was added dropwise under stirring. The mixture was stirred at $90\text{ }^\circ\text{C}$ for a further 12 h and allowed to cool down to room temperature. After that, deionized water (10 ml) was added to the reaction. The mixture was stirred for another 20 min. The red mixture was extracted by CH_2Cl_2 until the CH_2Cl_2 layer turned pale yellow. Then, the CH_2Cl_2 solution was dried over anhydrous MgSO_4 and filtered. The solution was concentrated and purified by column chromatography (silica) with 20 : 1 petrol/ethyl acetate as the eluent ($R_f = 0.8$),



Scheme 1 Synthetic procedures used in the preparation of LA and LA(Ln(III)) complexes.



Scheme 2 Synthetic procedures used in the preparation of LB and LB-Ln(III) complexes.

obtaining **A** (0.21 g, 62%) as an orange-red solid: mp $101\text{--}102\text{ }^\circ\text{C}$; ESI(+)-MS (m/z , methanol) = 224.1; ^1H NMR (400 MHz, CDCl_3) δ 8.13 (d, $J = 8.6\text{ Hz}$, 2H), 8.02–7.95 (m, 4H), 7.55 (d, $J = 7.2\text{ Hz}$, 3H), 2.68 (s, 3H).

Synthesis of 4-dimethylamino-4'-acetyl-azobenzene (B).⁶⁶ 4-Aminoacetophenone (0.83 g, 5.0 mmol) was dissolved in a HCl solution (5.0 mL, 3.0 mol L^{-1}). A solution of sodium nitrite (0.38 g, 5.5 mmol) in distilled water (5.0 mL) was prepared in a test tube and added dropwise to the acidic solution of 4-aminoacetophenone over 5 min at $0\text{ }^\circ\text{C}$. The mixture was stirred at $0\text{ }^\circ\text{C}$ for 30 min. *N,N*-Dimethylphenylamine (0.61 g, 5.0 mmol) was dissolved in 3 mL acetic acid and cooled to $0\text{ }^\circ\text{C}$, and the solution was added slowly to the above aryldiazonium salt solution at $0\text{ }^\circ\text{C}$. The resultant colored mixture was precipitated by addition of NaOH solution (20%). After the pH reached 7–8, the solution was stirred for a further 2 h at $0\text{ }^\circ\text{C}$. The precipitate was washed with 1 : 1 ethanol/water and recrystallized with acetone, generating a red solid (0.81 g, 61%); mp $173\text{--}175\text{ }^\circ\text{C}$; ESI(+)-MS (m/z , methanol) = 268.2; ^1H NMR (400 MHz, CDCl_3) δ 8.06 (d, $J = 8.4\text{ Hz}$, 2H), 7.93 (dd,

$J = 12.6, 8.8$ Hz, 4H), 6.77 (d, $J = 8.9$ Hz, 2H), 3.12 (s, 6H), 2.64 (s, 3H).

Synthesis of 4,4,5,5,6,6,6-heptafluoro-1-azobenzene-1,3-hexanedione (LA).⁶⁷ Sodium hydride (0.13 g, 5.5 mmol) and methyl heptafluorobutyrate (1.25 g, 5.5 mmol) were dissolved in dry ether (10 ml). The solution was stirred at 0–5 °C for 30 min. Then compound **A** (1.12 g, 5.0 mmol) was added to the above solution. The mixture was further stirred for 16 h at room temperature. A few drops of dilute sulfuric acid were added to the solution, which was further washed with water (3 × 15 mL). The resultant solution was separated and dried with anhydrous MgSO₄. Removal of the ether afforded a crude product, which was purified by recrystallization with ethanol to give a solid bright yellow pure product (1.41 g, 67%): mp 99–100 °C; ESI(+)-MS (m/z , methanol) = 421.2; ¹H NMR (400 MHz, CDCl₃) δ 15.25 (bs, 1H), 8.13 (d, $J = 8.6$ Hz, 2H), 8.08–7.93 (m, 4H), 7.55–7.50 (m, 3H), 6.68 (s, 1H); FT-IR (KBr, cm⁻¹) 3440 (s, O–H), 2922 (w, C–H), 1635 (s, C=O), 1516 (m, N=N), 1349 (s, C–N), 1240 (s, C–F), 1128 (s, C–O), 889, 797, 750, 691 (m, Ph–H); Elemental analysis (%) calculated for C₁₈H₁₁F₇N₂O₂: C, 51.44; H, 2.64; N, 6.67. Found: C, 51.53; H, 2.75; N, 6.61.

Synthesis of 4,4,5,5,6,6,6-heptafluoro-1-(4-dimethylamino)azobenzene-1,3-hexanedione (LB).⁶⁷ Sodium hydride (0.13 g, 5.5 mmol) and methyl heptafluorobutyrate (1.25 g, 5.5 mmol) were dissolved in dry ether (6.5 ml). The solution was stirred at 0–5 °C for 30 min. Then **B** (1.33 g, 5.0 mmol) was added to the above solution and the mixture was further stirred for 16 h at room temperature. After the addition of a few drops of dilute sulfuric acid, the solution was washed with water (3 × 15 mL), separated and dried with anhydrous MgSO₄. The mixture was concentrated and purified by column chromatography (silica) with 8 : 1 petrol/ethyl acetate as the eluent ($R_f = 0.7$), giving a pure deep red solid product (0.97 g, 42%): mp 145–147 °C; ESI(+)-MS (m/z , methanol) = 464.2; ¹H NMR (400 MHz, CDCl₃) δ 15.36 (s, 1H), 8.08 (d, $J = 8.3$ Hz, 2H), 7.96 (t, $J = 12.1$ Hz, 4H), 6.79 (d, $J = 8.0$ Hz, 2H), 6.66 (s, 1H), 3.13 (s, 6H); FT-IR (KBr, cm⁻¹) 3437 (s, O–H), 2922 (m, C–H), 1596 (s, C=O), 1518 (m, N=N), 1448 (m, C=C), 1366 (m, C–N), 1231 (s, C–F), 1141 (s, C–O), 885, 804, 744, 695 (m, Ph–H); Elemental analysis (%) calculated for C₂₀H₁₆F₇N₃O₂: C, 51.84; H, 3.48; N, 9.07. Found: C, 51.94; H, 3.95; N, 9.01.

Synthesis of Ln(III) complexes 1–8⁶⁸

General procedure. **LA** (or **LB**) (0.20 mmol) and NaOH (0.23 mmol) were dissolved in hot ethanol (10 mL) and water (1 mL). After the above solution was cooled down to room temperature, LnCl₃·6H₂O (0.067 mmol) in ethanol (10 mL) was added dropwise and the mixture was further stirred for 24 h (Schemes 1 and 2). The precipitate formed after the addition of water was filtered, recrystallized from 95% ethanol and dried in vacuum.

La(LA)₃(H₂O)₂, yellow solid (yield = 92%); mp 131–132 °C; ¹H NMR (400 MHz, CDCl₃) δ 8.36–8.18 (m, 18H), 7.49 (s, 9H), 6.68 (s, 3H); FT-IR (KBr, cm⁻¹) 3448 (s, O–H), 2915 (w, C–H), 1634 (s, C=O), 1524 (m, N=N), 1348 (m, C–N), 1225 (m, C–F),

1116 (m, C–O), 896, 797, 753, 694 (m, Ph–H); Elemental analysis (%) calculated for C₅₄H₃₄LaF₂₁N₆O₈: C, 45.27; H, 2.39; N, 5.87; Found: C, 45.21; H, 2.38; N, 5.86.

Eu(LA)₃(H₂O)₂, orange solid (yield = 95%); mp 128–130 °C; ¹H NMR (400 MHz, DMSO-*d*₆) δ 7.84 (s, 9H), 7.67–7.54 (m, 15H), 7.00 (s, 3H); 4.77 (s, 3H); FT-IR (KBr, cm⁻¹) 3434 (s, O–H), 2920 (w, C–H), 1616 (s, C=O), 1523 (m, N=N), 1486 (w, C=C), 1346 (m, C–N), 1227 (s, C–F), 1116 (m, C–O), 894, 791, 749, 692 (m, Ph–H); Elemental analysis (%) calculated for C₅₄H₃₄EuF₂₁N₆O₈: C, 4.86; H, 2.37; N, 5.81; Found: C, 43.45; H, 2.45; N, 5.75.

Gd(LA)₃(H₂O)₂, yellow solid (yield = 94%); mp 130–132 °C; FT-IR (KBr, cm⁻¹) 3448 (s, O–H), 2912 (w, C–H), 1618 (s, C=O), 1523 (m, N=N), 1485 (m, C=C), 1346 (m, C–N), 1226 (s, C–F), 1116 (s, C–O), 891, 791, 749, 692 (m, Ph–H); Elemental analysis (%) calculated for C₅₄H₃₄GdF₂₁N₆O₈: C, 44.70; H, 2.36; N, 5.79; Found: C, 44.74; H, 2.62; N, 5.78. (No NMR data due to the paramagnetic properties of the Gd(III) ion.)

Yb(LA)₃(H₂O)₂, yellow solid (yield = 90%); mp 131–133 °C; ¹H NMR (400 MHz, CDCl₃) δ 9.79 (s, 6H), 8.78 (s, 6H), 8.44 (s, 6H), 7.84 (s, 9H), 6.72 (s, 3H); FT-IR (KBr, cm⁻¹) 3449 (s, O–H), 2920 (w, C–H), 1617 (s, C=O), 1573 (m, C=C), 1521 (m, N=N), 1343 (m, C–N), 1227 (s, C–F), 1140 (s, C–O), 891, 792, 753, 691 (m, Ph–H); Elemental analysis (%) calculated for C₅₄H₃₄YbF₂₁N₆O₈: C, 44.21; H, 2.34; N, 5.73; Found: C, 44.04; H, 2.41; N, 5.68. Orange plate crystals were obtained by slow evaporation of ethanol solution. Ethanol substituted the coordinated water molecule in the crystal structure to give **Yb(LA)₃(CH₃CH₂OH)₂**.

La(LB)₃(H₂O)₂, deep red solid (yield = 89%); mp 260–263 °C; ¹H NMR (400 MHz, DMSO-*d*₆) δ 8.04 (s, 6H), 7.77 (dd, $J = 18.0, 8.6$ Hz, 12H), 6.82 (d, $J = 9.1$ Hz, 6H), 6.36 (s, 3H), 3.07 (s, 18H); FT-IR (KBr, cm⁻¹) 3439 (s, O–H), 2920 (w, C–H), 1605 (s, C=O), 1573 (m, C=C), 1519 (m, N=N), 1366 (m, C–N), 1229 (m, C–F), 1139 (s, C–O), 892, 791, 750, 622 (m, Ph–H); Elemental analysis (%) calculated for C₆₀H₄₉LaF₂₁N₉O₈: C, 46.14; H, 3.16; N, 8.07; Found: C, 45.68; H, 3.51; N, 7.91.

Eu(LB)₃(H₂O)₂, deep red solid (yield = 92%); mp 250–253 °C; ¹H NMR (400 MHz, CDCl₃) δ 8.15 (d, $J = 8.5$ Hz, 9H), 8.06–8.01 (m, 9H), 7.32 (s, 6H), 7.25–7.23 (m, 3H), 2.71 (s, 18H); FT-IR (KBr, cm⁻¹) 3437 (s, O–H), 2917 (w, C–H), 1606 (s, C=O), 1571 (m, C=C), 1518 (m, N=N), 1366 (m, C–N), 1226 (s, C–F), 1141 (s, C–O), 894, 791, 750, 618 (m, Ph–H); Elemental analysis (%) calculated for C₅₄H₄₉EuF₂₁N₆O₈: C, 45.75; H, 3.14; N, 8.00; Found: C, 45.31; H, 3.43; N, 7.92. Orange plate crystals were obtained by slow evaporation of ethanol and acetone mixed solution. Ethanol substituted the coordinated water molecule in the crystal structure to give **Eu(LB)₃(CH₃CH₂OH)(H₂O)**.

Gd(LB)₃(H₂O)₂, deep red solid (yield = 89%); mp 250–253 °C; FT-IR (KBr, cm⁻¹) 3449 (s, O–H), 2918 (m, C–H), 1605 (s, C=O), 1571 (m, C=C), 1518 (m, N=N), 1366 (m, C–N), 1227 (s, C–F), 1141 (s, C–O), 894, 798, 750, 619 (m, Ph–H); Elemental analysis (%) calculated for C₅₄H₄₉GdF₂₁N₆O₈: C, 45.60; H, 3.13; N, 7.98; Found: C, 45.66; H, 3.04; N, 7.91.

(No NMR data due to the paramagnetic properties of the Gd(III) ion.)

Yb(LB)₃(H₂O)₂, deep red solid (yield = 87%); mp 263–265 °C; ¹H NMR (400 MHz, CDCl₃) δ 10.05 (s, 6H), 8.97 (s, 6H), 8.65 (s, 6H), 7.11 (d, *J* = 7.0 Hz, 6H), 6.87 (s, 3H), 3.35 (s, 18H); FT-IR (KBr, cm⁻¹) 3443 (s, O–H), 2917 (w, C–H), 1607 (s, C=O), 1571 (m, C=C), 1521 (m, N=N), 1366 (m, C–N), 1230 (s, C–F), 1140 (s, C–O), 820, 791, 750, 620 (m, Ph–H); Elemental analysis (%) calculated for C₆₀H₄₉YbF₂₁N₉O₈: C, 45.15; H, 3.09; N, 7.90; Found: C, 45.56; H, 3.15; N, 7.85. Orange plate crystals were obtained by slow evaporation of ethanol solution. Ethanol substituted the coordinated water molecules in the crystal structure to give **Yb(LB)₃(CH₃CH₂OH)₂**.

PMMA thin film preparation

Complexes were made into thin films using PMMA as the polymer matrix. 100.0 mg of PMMA was dissolved in 20.0 mL chloroform with mild sonication for 15 min. 5.0 mg of the complex was added to the above solution and sonicated mildly. The polymer thin film with approximately the same thickness was coated on a 12 mm × 45 mm Quartz plate substrate.

Measurement of photoisomerization quantum yields

365 nm UV light was obtained from a ZF-2 UV analyzer (Shanghai Yihui). For the *cis*-to-*trans* reverse reactions, visible light irradiation was from a 300 W Xe lamp (PLS-SXE300CUV). The 450 nm light was isolated by a sharp cut filter. A 10 mm light path-length quartz cell was used for the isomerization measurements. The light intensity was measured by a UV-A radiation meter (optical electrical apparatus factory of Beijing Normal University). The sample concentration was 2.0 × 10⁻⁵ mol L⁻¹ for all complexes. The quantum yield for photoisomerization is evaluated using eqn (1):^{61,69}

$$\Phi = k_0 \frac{1}{I_0} \frac{1}{1 - 10^{-\epsilon cl}} \quad (1)$$

where k_0 is a zero-order rate constant for the decrease of the initial isomer concentration in mol L⁻¹ s⁻¹, I_0 is the intensity of incident irradiation light in einstein L⁻¹ s⁻¹, ϵ is the extinction coefficient in L mol⁻¹ cm⁻¹ at the irradiation wavelength of the solution, c is the concentration of this solution in mol L⁻¹, and l is the path length of the light through the sample in cm. The *trans*-to-*cis* photoisomerization obeyed first-order kinetics, with the isomerization rate constant, k_{iso} , being calculated from the change in absorbance at a certain wavelength with time using eqn (2):^{39,40}

$$\ln \frac{A_\infty - A_0}{A_\infty - A_t} = k_{\text{iso}} t \quad (2)$$

where A_t , A_0 , and A_∞ denote the absorbance at time t , zero time and at the end of the reaction, respectively.

The uncertainty of the quantum yields and the rate constants for all compounds were calculated according to three independent replicates performed for each concentration.

Time dependent density functional theory (TD-DFT) calculations

DFT calculations were performed with the three-parametrized Becke–Lee–Yang–Parr (B3LYP) hybrid exchange–correlation functional and 6-31+G(d) basis set by using the Gaussian 09 program.⁷⁰ Low-lying singlet and triplet excitation energies were calculated at the optimized geometries by TD-DFT with the same basis set. The geometries of these compounds were optimized by the DFT(B3LYP) method without considering the solvent effect.

Structure determination of Yb(LA)₃, Eu(LB)₃, Yb(LB)₃ by the X-ray diffraction

The X-ray diffraction data were collected on a Bruker SMART Apex CCD diffractometer equipped with graphite-monochromatic MoK α (λ = 0.71073 Å) radiation using an ω scan mode at 173(2) K. The crystal data integration and reduction steps were performed using the SAINT software. Lorentz-polarization and empirical absorption corrections were applied to the data. The structure was solved by direct methods with SHELXS-97 and refined by full-matrix least-squares calculations with SHELXL-97 based on F^2 .⁷¹ All non-hydrogen atoms were refined anisotropically. Treatment of hydrogen atoms in the least-squares refinement resulted in different data, some of them were constrained, the others were independent. For the constrained data, hydrogen atoms were located at the calculated positions. Three –C₃F₇ groups in the compounds were seriously disordered and they were restrained because of the high displacement parameters. The “simu, delu, dfix and isor” restraints were used in the refinement of –C₃F₇ groups to ensure reasonable bonds and conformation. Some of the C–F distances were restrained to their ideal values and F–F distances were restrained to be similar to regularize the angles. One of the –C₃F₇ groups in molecules Eu(LB)₃, Yb(LA)₃ and the coordinated solvent ethanol in the molecule Yb(LB)₃ were found to be rotationally disordered around two independent orientations. The occupancy of disordered fluorines and ethanol at two orientations was refined by using the PART command in SHELXL2014. Crystallographic details for complexes Yb(LA)₃, Eu(LB)₃ and Yb(LB)₃ are summarized in Table 1. Data for the crystal structures of complexes Yb(LA)₃, Eu(LB)₃ and Yb(LB)₃ have been deposited at the Cambridge Crystallographic Data Centre (CCDC 1422641 for Eu(LB)₃, 1422642 for Yb(LA)₃, and 1422643 for Yb(LB)₃).

Conclusions

In summary, we have synthesized and characterized eight lanthanide tris- β -diketonate complexes functionalized with the azobenzene group. Among these complexes, we obtained three crystal structures. They have very similar structures and all three complexes crystallize in the triclinic $P\bar{1}$ space group. The lanthanide(III) ion is eight-coordinated to six oxygen atoms from the three β -diketonate ligands and two oxygen atoms from solvent molecules, forming a trigonal dodecahedron

coordination geometry. The photoisomerization properties of the complexes have been investigated in detail. All the complexes are able to undergo reversible *trans*-to-*cis* photoisomerization in different organic solvents as well as in solid PMMA film. The LA-Ln(III) complexes bearing azobenzene groups without a donor substituent show better reversible *trans*-to-*cis* photoisomerization compared with the LB-Ln(III) complexes. Although the luminescence properties of the LA-Ln(III) and LB-Ln(III) complexes were not observed due to the resonance level of Ln(III) being higher than that of the ligands, it is remarkable to find that the newly designed complexes possess the unique properties of fast *trans*-to-*cis* photoisomerization, large extinction coefficient and high fatigue resistance both in solution and in solid PMMA film. We believe that this novel design of the complexes, together with the influence of the electron donor, opens a new perspective for the development of photoisomerization of azobenzene-derived Ln(III) complexes and offers great flexibility and options for the rational design of ligands, which, in turn, will facilitate development of photoisomerization. We are currently focusing on the studies of this modified system in which the photoisomerization is accompanied with luminescence properties via properly designed azobenzene derived β -diketones and might be applicable to optical devices, photonic memory and biological photosensing fields.

Acknowledgements

We are grateful for financial support by the National Natural Science Foundation of China (Grant No. 21271150 and 21273175) and the Natural Science Foundation of Fujian province (Grant No. 2015J01060).

Notes and references

- C. Dugave and L. Demange, *Chem. Rev.*, 2003, **103**, 2475–2532.
- H. M. Bandara and S. C. Burdette, *Chem. Soc. Rev.*, 2012, **41**, 1809–1825.
- M. M. Russew and S. Hecht, *Adv. Mater.*, 2010, **22**, 3348–3360.
- S. Samanta, A. A. Beharry, O. Sadovski, T. M. McCormick, A. Babalhavaeji, V. Tropepe and G. A. Woolley, *J. Am. Chem. Soc.*, 2013, **135**, 9777–9784.
- R. H. El Halabieh, O. Mermut and C. J. Barrett, *Pure Appl. Chem.*, 2004, **76**, 1445–1465.
- P. P. Lima, M. M. Nolasco, F. A. A. Paz, R. A. S. Ferreira, R. L. Longo, O. L. Malta and L. D. Carlos, *Chem. Mater.*, 2013, **25**, 586–598.
- D. Bleger, J. Schwarz, A. M. Brouwer and S. Hecht, *J. Am. Chem. Soc.*, 2012, **134**, 20597–20600.
- V. Torres-Zuniga, O. G. Morales-Saavedra, E. Rivera, R. Castaneda-Guzman, J. G. Banuelos and R. Ortega-Martinez, *J. Sol-Gel Sci. Technol.*, 2010, **56**, 7–18.
- S. W. Magennis, F. S. Mackay, A. C. Jones, K. M. Tait and P. J. Sadler, *Chem. Mater.*, 2005, **17**, 2059–2062.
- K. Kinbara and T. Aida, *Chem. Rev.*, 2005, **105**, 1377–1400.
- T. Hugel, N. B. Holland, A. Cattani, L. Moroder, M. Seitz and H. E. Gaub, *Science*, 2002, **296**, 1103–1106.
- K. Ichimura, *Chem. Rev.*, 2000, **100**, 1847–1873.
- H. A. Haque, S. Kakehi, M. Hara, S. Nagano and T. Seki, *Langmuir*, 2013, **29**, 7571–7575.
- S. Kubo, Z. Z. Gu, K. Takahashi, A. Fujishima, H. Segawa and O. Sato, *J. Am. Chem. Soc.*, 2004, **126**, 8314–8319.
- A. Miniewicz, J. Girones, P. Karpinski, B. Mossety-Leszczak, H. Galina and M. Dutkiewicz, *J. Mater. Chem. C*, 2014, **2**, 432–440.
- S. Pieraccini, S. Masiero, G. P. Spada and G. Gottarelli, *Chem. Commun.*, 2003, 598–599.
- P. C. Che, Y. N. He and X. G. Wang, *Macromolecules*, 2005, **38**, 8657–8663.
- B. Rajashekar, S. Limbu, K. Aditya, G. Nageswara Rao and S. Siva Sankara Sai, *Photochem. Photobiol. Sci.*, 2013, **12**, 1780–1786.
- A. Natansohn and P. Rochon, *Chem. Rev.*, 2002, **102**, 4139–4175.
- Y. L. Yu, M. Nakano and T. Ikeda, *Nature*, 2003, **425**, 145–145.
- J. Henzl, M. Mehlhorn, H. Gawronski, K. H. Rieder and K. Morgenstern, *Angew. Chem., Int. Ed.*, 2006, **45**, 603–606.
- K. Namiki, A. Sakamoto, M. Murata, S. Kume and H. Nishihara, *Chem. Commun.*, 2007, 4650–4652.
- K. Ichimura, S. K. Oh and M. Nakagawa, *Science*, 2000, **288**, 1624–1626.
- Y. R. Choi, G. C. Kim, H. G. Jeon, J. Park, W. Namkung and K. S. Jeong, *Chem. Commun.*, 2014, **50**, 15305–15308.
- A. Cattani-Scholz, C. Renner, C. Cabrele, R. Behrendt, D. Oesterhelt and L. Moroder, *Angew. Chem., Int. Ed.*, 2002, **41**, 289–291.
- H. Asanuma, X. Liang, H. Nishioka, D. Matsunaga, M. Liu and M. Komiyama, *Nat. Protoc.*, 2007, **2**, 203–212.
- F. Wang, X. Liu and I. Willner, *Angew. Chem., Int. Ed.*, 2015, **54**, 1098–1129.
- Z. Mahimwalla, K. G. Yager, J. Mamiya, A. Shishido, A. Priimagi and C. J. Barrett, *Polym. Bull.*, 2012, **69**, 967–1006.
- J. Park, L. B. Sun, Y. P. Chen, Z. Perry and H. C. Zhou, *Angew. Chem., Int. Ed.*, 2014, **53**, 5842–5846.
- S. Kume, M. Kurihara and H. Nishihara, *Chem. Commun.*, 2001, 1656–1657.
- M. Torrents, M. Ortiz, A. P. Turner, V. Beni and C. K. O'Sullivan, *Chem. – Eur. J.*, 2015, **21**, 671–681.
- F. A. Garlich-Zschoche and K. H. Dotz, *Organometallics*, 2007, **26**, 4535–4540.
- R. Singh, M. Ahmad and P. K. Bharadwaj, *Cryst. Growth Des.*, 2012, **12**, 5025–5034.
- T. Yutaka, I. Mori, M. Kurihara, N. Tamai and H. Nishihara, *Inorg. Chem.*, 2003, **42**, 6306–6313.
- J. F. Yan, D. Q. Lin, X. G. Wang, K. Q. Wu, L. L. Xie and Y. F. Yuan, *Chem. – Asian J.*, 2015, **10**, 614–621.

- 36 A. Sakamoto, A. Hirooka, K. Namiki, M. Kurihara, M. Murata, M. Sugimoto and H. Nishihara, *Inorg. Chem.*, 2005, **44**, 7547–7558.
- 37 I. Guezguez, A. Ayadi, K. Ordon, K. Iliopoulos, D. G. Branza, A. Migalska-Zalas, M. Makowska-Janusik, A. El-Ghayoury and B. Sahraoui, *J. Phys. Chem. C*, 2014, **118**, 7545–7553.
- 38 A. Telleria, J. Pérez-Miqueo, A. Altube, E. García-Lecina, A. de Cózar and Z. Freixa, *Organometallics*, 2015, **34**, 5513–5529.
- 39 T. Yutaka, I. Mori, M. Kurihara, J. Mizutani, K. Kubo, S. Furusho, K. Matsumura, N. Tamai and H. Nishihara, *Inorg. Chem.*, 2001, **40**, 4986–4995.
- 40 T. Yutaka, M. Kurihara, K. Kubo and H. Nishihara, *Inorg. Chem.*, 2000, **39**, 3438–3439.
- 41 T. Yutaka, I. Mori, M. Kurihara, J. Mizutani, N. Tamai, T. Kawai, M. Irie and H. Nishihara, *Inorg. Chem.*, 2002, **41**, 7143–7150.
- 42 V. Guerchais and H. Le Bozec, *Top. Organomet. Chem.*, 2010, **28**, 171–225.
- 43 A. Fihey, A. Perrier, W. R. Browne and D. Jacquemin, *Chem. Soc. Rev.*, 2015, **44**, 3719–3759.
- 44 Y. J. Lin, F. Zou, S. G. Wan, J. Ouyang, L. R. Lin and H. Zhang, *Dalton Trans.*, 2012, **41**, 6696–6706.
- 45 J. Shi, Y. J. Hou, W. Y. Chu, X. H. Shi, H. Q. Gu, B. L. Wang and Z. Z. Sun, *Inorg. Chem.*, 2013, **52**, 5013–5022.
- 46 Y. J. Hou, J. Shi, W. Y. Chu and Z. Z. Sun, *Eur. J. Inorg. Chem.*, 2013, 3063–3069.
- 47 J. L. Lunkley, D. Shirovani, K. Yamanari, S. Kaizaki and G. Muller, *Inorg. Chem.*, 2011, **50**, 12724–12732.
- 48 J. P. Martins, P. Martin-Ramos, C. Coxa, A. L. Alvarez, L. C. Pereira, R. Diaz, J. Martin-Gil and M. R. Silva, *Mater. Chem. Phys.*, 2014, **147**, 1157–1164.
- 49 A. Lannes, M. Intissar, Y. Suffren, C. Reber and D. Luneau, *Inorg. Chem.*, 2014, **53**, 9548–9560.
- 50 R. K. Mahajan, I. Kaur, R. Kaur, S. Uchida, A. Onimaru, S. Shinoda and H. Tsukube, *Chem. Commun.*, 2003, 2510–2510.
- 51 H. Tsukube, S. Shinoda, J. Uenishi, T. Kanatani, H. Itoh, M. Shiode, T. Iwachido and O. Yonemitsu, *Inorg. Chem.*, 1998, **37**, 1585–1591.
- 52 R. K. Mahajan, I. Kaur, R. Kaur, A. Onimaru, S. Shinoda and H. Tsukube, *Anal. Chem.*, 2004, **76**, 7354–7359.
- 53 J. Sun, B. Song, Z. Ye and J. Yuan, *Inorg. Chem.*, 2015, **54**, 11660–11668.
- 54 A. J. Roche, S. A. Rabinowitz and K. A. Cox, *Tetrahedron: Asymmetry*, 2013, **24**, 1382–1388.
- 55 L. Di Bari, M. Lelli, G. Pintacuda and P. Salvadori, *Chirality*, 2002, **14**, 265–273.
- 56 A. Valore, E. Cariati, S. Righetto, D. Roberto, F. Tessore, R. Ugo, I. L. Fragala, M. E. Fragala, G. Malandrino, F. De Angelis, L. Belpassi, I. Ledoux-Rak, K. H. Thi and J. Zyss, *J. Am. Chem. Soc.*, 2010, **132**, 4966–4970.
- 57 L. N. Sun, Y. N. Qiu, T. Liu, J. Z. Zhang, S. Dang, J. Feng, Z. J. Wang, H. J. Zhang and L. Y. Shi, *ACS Appl. Mater. Interfaces*, 2013, **5**, 9585–9593.
- 58 A. W. Woodward, A. Frazer, A. R. Morales, J. Yu, A. F. Moore, A. D. Campiglia, E. V. Jucov, T. V. Timofeeva and K. D. Belfield, *Dalton Trans.*, 2014, **43**, 16626–16639.
- 59 S. V. Eliseeva, D. N. Pleshkov, K. A. Lyssenko, L. S. Lepnev, J. C. Bunzli and N. P. Kuzmina, *Inorg. Chem.*, 2010, **49**, 9300–9311.
- 60 J. C. G. Bunzli, *Chem. Rev.*, 2010, **110**, 2729–2755.
- 61 P. Sierocki, H. Maas, P. Dragut, G. Richardt, F. Vogtle, L. Cola, F. A. M. Brouwer and J. I. Zink, *J. Phys. Chem. B*, 2006, **110**, 24390–24398.
- 62 L. R. Lin, Q. J. Xu, X. Wu, R. B. Huang and L. S. Zheng, *J. Fluoresc.*, 2011, **21**, 1319–1324.
- 63 S. I. Kazantseva and V. V. Levin, *J. Struct. Chem.*, 1973, **14**(3), 505–506.
- 64 S. Sato and M. Wada, *Bull. Chem. Soc. Jpn.*, 1970, **43**, 1955–1962.
- 65 J. D. Badjić and N. M. Kostić, *J. Mater. Chem.*, 2001, **11**, 408–418.
- 66 K. Haghbeen and E. W. Tan, *J. Org. Chem.*, 1998, **63**, 4503–4505.
- 67 S. Büttner, M. Lubbe, H. Reinke, C. Fischer and P. Langer, *Tetrahedron*, 2008, **64**, 7968–7976.
- 68 H. F. Li, P. F. Yan, P. Chen, Y. Wang, H. Xu and G. M. Li, *Dalton Trans.*, 2012, **41**, 900–907.
- 69 J. Saltiel, Y. X. Zhang and D. F. Sears, *J. Am. Chem. Soc.*, 1997, **119**, 11202–11210.
- 70 M. J. Frisch, G. W. Trucks, H. B. Schlegel, G. E. Scuseria, M. A. Robb, J. R. Cheeseman, G. B. Scalmani, V. B. Mennucci, G. A. Petersson, H. Nakatsuji, M. Caricato, X. Li, H. P. Hratchian, A. F. Izmaylov, J. Bloino, G. Zheng, J. L. Sonnenberg, M. Hada, M. Ehara, K. Toyota, R. Fukuda, J. Hasegawa, M. Ishida, T. Nakajima, Y. Honda, O. Kitao, H. Nakai, T. Vreven, J. A. Montgomery, J. E. Peralta, F. Ogliaro, M. Bearpark, J. J. Heyd, E. Brothers, K. N. Kudin, V. N. Staroverov, R. Kobayashi, J. Normand, K. Raghavachari, A. Rendell, J. C. Burant, S. S. Iyengar, J. Tomasi, M. Cossi, N. Rega, N. J. Millam, M. Klene, J. E. Knox, J. B. Cross, V. Bakken, C. Adamo, J. Jaramillo, R. Gomperts, R. E. Stratmann, O. Yazyev, A. J. Austin, R. Cammi, C. Pomelli, J. W. Ochterski, R. L. Martin, K. Morokuma, V. G. Zakrzewski, G. A. Voth, P. Salvador, J. J. Dannenberg, S. Dapprich, A. D. Daniels, Ö. Farkas, J. B. Foresman, J. V. Ortiz, J. Cioslowski and D. J. Fox, Gaussian, Inc., Wallingford CT, 2009.
- 71 G. M. Sheldrick, *SHELXS 97 and SHELXL 97*, University of Göttingen, Germany, 1997.